2026 IEEE/SICE International Symposium on System Integration (SII)
January 11-14, 2026. Cancún, México

Position and stiffness control based on a mechanical-equilibrium model for antagonistic joints using hyper-extension actuators

A. Irie, A. Kobayashi, R. Sawahashi, F. Ito, R. Nishihama, and T. Nakamura, *Member, IEEE*

Abstract— **In this study, we develop an antagonistic joint using a hyper-extension actuator for the development of robots that can perform human-like movements that are smooth and flexible. Previous antagonistic joints using pneumatic artificial muscles could not maintain joint rigidity when no air pressure was applied. The hyper-extension actuator greatly elongates when air pressure is applied and has a small radial-expansion rate. By applying this actuator to the antagonistic joint, joint stiffness can be maintained even without air-pressure application. The developed antagonistic joint can achieve a target joint angle range of -90–90 deg and joint stiffness of 0.1, 0.2, and 0.3 Nm/rad by controlling the applied pressure to the actuator, as defined by a model. The pressure-control performance of the joint angles and stiffness is verified using an actual device. The results demonstrate that the expected and measured values are in agreement.**

I. INTRODUCTION

Recently, the development of robots that can coexist with humans has attracted significant attention. Robots play active roles in many fields, including industrial robots used in factories [1, 2] and human power-assist suits [3, 4]. To realize these robots, delicate, skillful, and smooth human movements must be achieved. One method that enables this is the use of an antagonistic joint. An antagonistic joint is a joint in which two muscles are arranged in pairs relative to the joint, and they work together to move the joint. A high or low tension in both muscles results in high or low joint stiffness, respectively. By freely controlling the stiffness, a back drive may be achieved [5], where the output joint moves in response to external forces, such as human movement. Therefore, robots capable of safe and flexible movements when operating near humans can be realized.

Robots with antagonistic joints have been developed using pneumatic artificial muscles [6-9], dielectric elastomers [10, 11], and motors [12, 13]. When developing robots aimed at human–robot collaboration, dielectric elastomers offer the advantage of easy control but are limited by low output and susceptibility to external forces. In contrast, motors have the advantage of high output, but pose safety risks when operating near humans owing to their high weight and large inertial forces. Therefore, the use of soft actuators, such as pneumatic artificial muscles, which are soft, impact-resistant, lightweight, and have a high output, is currently attracting attention.

In addition to the commonly used McKibben muscles [9, 14], straight-fiber-type pneumatic artificial muscles have also been developed [15, 16]. In the structure of straight-fiber-type pneumatic artificial muscles, the reinforcement fibers align only in the axial direction are enclosed in a rubber tube. When pneumatic pressure is applied, the reinforcement fibers constrain the tube, causing it to expand radially and contract axially. Compared to conventional McKibben muscles, they offer advantages such as higher contraction rates, greater contraction forces, and longer lifespans. To date, this artificial muscle has been used to develop manipulators with antagonistic joints [17] and walking-assistance devices [18, 19]. However, the application of straight-fiber-type pneumatic artificial muscles may be challenging. When no air pressure is applied, they cannot exert tension or maintain joint stiffness. In addition, when air pressure is applied, they expand radially; therefore, they must be designed with a predefined space for expansion, which makes miniaturization difficult.

Therefore, this study focuses on a hyper-extension pneumatic actuator (HEA) [20] with artificial-muscle characteristics. The HEA contains spiral-shaped long fibers and short fiber-oriented threads inside a natural rubber tube. By utilizing this structure, the expansion of the rubber is suppressed, and the stress concentration on the rubber is minimized. Consequently, when pneumatic pressure is applied, the actuator exhibits minimal radial expansion (radial expansion rate of less than 25 %), while achieving a significant axial elongation (maximum elongation of 520 %). Because of its large elongation displacement, the actuator can generate a force specifically in the desired direction. Compared with straight-fiber-type pneumatic artificial muscles, the HEA is a lightweight, compact, and high-output actuator. However, no antagonistic joints have been developed based on mechanical-equilibrium models using an HEA. The advantages and characteristics of using an HEA in antagonistic joints are as follows:

- The long stroke allows for a wide range of operations.
- When the pressure is low, the joint reaches its high stiffness, which helps reduce energy consumption during long-duration carrying tasks and so on.
- Because it does not expand radially when air pressure is applied, miniaturization is possible.

This study develops a robot capable of smooth and flexible human-like movements by creating an antagonistic joint (Fig. 1) based on a mechanical-equilibrium model using an HEA. The proposed device uses two HEA units, each of which is

A. Irie, A. Kobayashi, R. Sawahashi, F. Ito, and T. Nakamura are with the Department of Precision Mechanics, Faculty of Science and Engineering, Chuo University, 1-13-27 Kasuga, Bunkyo-Ku, Tokyo, 112-8551, Japan (corresponding author to provide e-mail: a21.xwmk@g.chuo-u.ac.jp).

R. Nishihama is with Research and Development Initiative, Chuo University, 1-13-27 Kasuga, Bunkyo-ku, Tokyo 112-8551, Japan (e-mail: nrie002l@g.chuo-u.ac.jp).

978-1-6654-5784-2/26/$31.00 ©2026 IEEE

pressurized with air to enable the free control of the joint angle and stiffness. In future, we aim to apply this mechanism

to assistive devices by operating it in accordance with human joint movements. In this study, we create a model for an antagonistic joint and determine the range of air pressures to be applied to the actuator to control the joint angle and stiffness through a simulation. Subsequently, we construct a prototype and verify whether the specified joint angle and stiffness can be output.

The remainder of this paper is organized as follows. Section II describes the characteristics of the HEA and operating principles of antagonistic joints using actuators. Section III describes the model for controlling an antagonistic joint that is manufactured based on a mechanical-equilibrium model using actuators. Section IV describes the simulations conducted to verify the accuracy of the model. Section V describes the motion system for operating an actual device using the control model. Section VI verifies whether the joint angle and stiffness are output as expected in the actual device.

II. ANTAGONISTIC JOINTS BASED ON A MECHANICAL-EQUILIBRIUM MODEL USING AN HEA

A. Overview

An antagonistic joint based on the mechanical-equilibrium model using the newly developed HEA is shown in Fig. 1. This device consists of two antagonistically arranged HEAs, arms, pulleys with bearings, wires, an aluminum frame, a rotary encoder (E6B2-CWZ6C, OMRON) to measure the joint angles via gears, an air-pressure sensor (ITV2050-312L, SMC) to measure the air pressure applied to the HEA, and a load cell (LUR-A-500NSA1, KYOWA) to measure the tensile force generated by the HEA. The joint angle is controlled by adjusting the air pressure applied to each actuator. Additionally, the joint stiffness can also be adjusted freely because this joint has variable stiffness.

B. HEA characteristics

Fig. 2 shows the displacement-tensile force characteristics of the HEA. These are the measurement results of the tensile force F [N] and displacement x [mm] during the 150-mm extension and contraction of the actuator without the application of air pressure. Five cycles of 50-mm extension, contraction, and extension were performed before the test to confirm that the elongation of the actuator had converged. Subsequently, the initial length of the actuator was measured and a basic characteristic test was performed.

For the range of 0–120 mm, which is used in the proposed antagonistic joint during the extension and contraction of the actuator, a linear approximation ($R^2 = 0.98$) was performed on the contraction results, and the following equation was obtained:

$$F = 1.1x \tag{1}$$

Based on Equation (1), the HEA has the characteristics of a typical spring ($k = 1.1$ N/mm). To simplify the model equation, a simple linear equation was used this time; however, by performing an approximation that accounts for hysteresis, it is possible to improve the accuracy of the performance.

C. Principle of antagonistic joint movement

Next, the operating principles of the antagonistic joint are explained. First, air pressure was applied to the actuator, and the wire was stretched to twice its length to prevent sagging. This state was considered as the initial position. Subsequently, the displacement was varied to control the joint angle by adjusting the applied air pressure. Similarly, joint stiffness was controlled by adjusting the applied air pressure. The

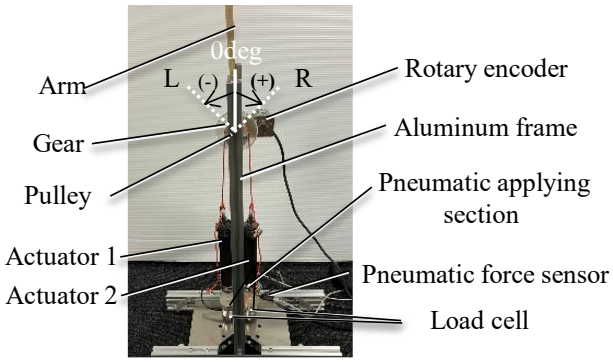

Figure 1. Antagonistic joint system with hyper-extension actuators.

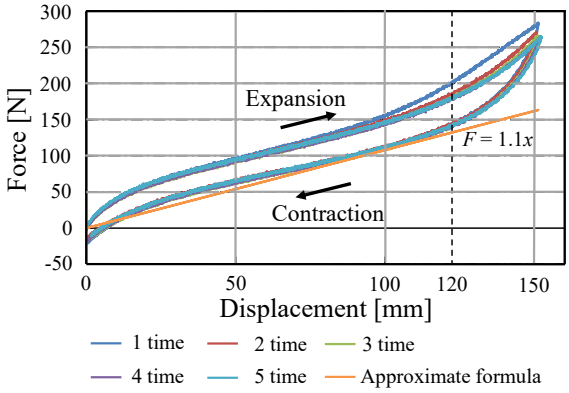

Figure 2. Force–pressure–displacement relationship of an HEA.

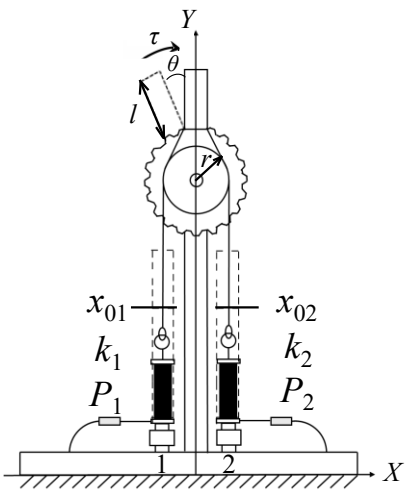

Figure 3. Antagonistic joint model.

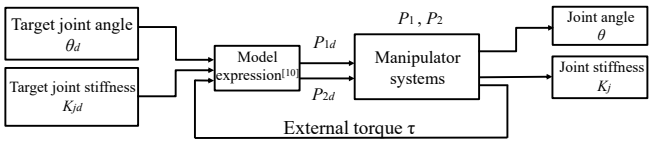

Figure 4. Block diagram.

characteristics of the antagonistic joint based on a mechanical-equilibrium model using the HEA are as follows:

- For the same angle, if the displacement from the unloaded state of the actuator is large, the joint stiffness is low; if the displacement is small, the joint stiffness is high.
- Maximum joint rigidity is achieved when no air pressure is applied.
- Because the length is shortest in the absence of a load, the wire connecting the actuator can operate without sagging.
- The extended state can be maintained even after the air pressure is released from the actuator.
- Pneumatic control to achieve variable rigidity is difficult.

Based on the above, we controlled antagonistic joints based on a mechanical-equilibrium model using an HEA by introducing the control model, which is described in the next section.

III. Control Method Based on Mechanical-Equilibrium Model

A. Control model

Fig. 3 shows a diagram of an antagonistic joint device based on a mechanical-equilibrium model using an HEA. The l in Fig. 3 is the arm length of 60 mm. Fig. 4 shows a block diagram of the control of the joint angle and stiffness of the device. The command applied pressure is determined, and the antagonistic joint is controlled by inputting the target joint stiffness and angle into the model.

The model was derived by referencing the model for an antagonistic joint based on a mechanical-equilibrium model using dielectric elastomers [10]. Using the relationship between the joint angle, displacement of the HEA that expands and contracts when air pressure is applied, and external torque, we derive an equation that includes the variables of displacement x_{P1} and x_{P2}, which expand and contract when air pressure is applied to actuators 1 (left side in Fig. 1) and 2 (right side), external torque τ, and target joint angle θ_d:

$$(k_1 + k_2)r\theta_d + \frac{\tau}{r} = k_1 x_{P1} - k_2 x_{P2} \tag{2}$$

Subsequently, we derive the joint-stiffness control equation. First, we calculate the stiffness of each joint based on the relationship between the air pressure applied to actuators 1 and 2 and the joint angle:

$$K_1 = k_1 - \frac{k_1 x_{P1}}{r\theta_d + x_{01}} \tag{3-1}$$

$$K_2 = k_2 - \frac{k_2 x_{P2}}{-r\theta_d + x_{02}} \tag{3-2}$$

We derive the relationship between the displacements x_{P1} and x_{P2} of the HEA, which expand and contract owing to air pressure, and the target joint stiffness K_{jd}.

$$K_{jd} = \left(k_1 - \frac{k_1 x_{P1}}{r\theta_d + x_{01}} + k_2 - \frac{k_2 x_{P2}}{-r\theta_d + x_{02}}\right) r^2 \tag{4}$$

Equations (2) and (4) are combined as they relate to the target joint stiffness K_{jd}, external torque τ, and target joint angle θ_d, with variables x_{P1} and x_{P2} and the target joint angle θ_d used to derive the equations. By dividing the displacements x_{P1} and x_{P2} by the cross-sectional areas A_1 and A_2 of the actuators, the applied pressures P_{1d} and P_{2d} on each actuator can be expressed using Equations (5) and (6), respectively:

$$P_{1d} = \frac{1}{A_1} \times \frac{r\theta_d + x_{01}}{a \times k_1 (x_{01} + x_{02})} \times \left\{(k_1 + k_2)x_{02} + \frac{\tau}{r} - \frac{K_{jd}}{r^2}(-r\theta + x_{02})\right\} \tag{5}$$

$$P_{2d} = \frac{1}{A_2} \times \frac{-r\theta_d + x_{02}}{a \times k_2 (x_{01} + x_{02})} \times \left\{(k_1 + k_2)x_{01} - \frac{\tau}{r} - \frac{K_{jd}}{r^2}(r\theta + x_{01})\right\} \tag{6}$$

Note that x_{01} and x_{02} are the initial displacements of the actuators, k_1 and k_2 are the spring constants of the actuators, r is the pulley radius, and a is the adjustment coefficient related to spring constants k_1 and k_2 when the actuators are extended. The target joint angle and stiffness were obtained by applying air pressure to each actuator.

Equations (5) and (6) represent the target values of the air pressure applied to each actuator. Equations (5) and (6) derive the air pressure from two parameters: the displacement and joint stiffness. The model consists of terms related to the cross-sectional area of the actuator, spring constant when the actuator is extended, spring force when the actuator is maximally extended, external force applied to the joint, and force output when the actuator is extended. The target air pressure applied to the actuator, calculated from the model, was input to a proportional solenoid valve via D/A conversion, and the air pressure applied by the compressor was controlled. The displacement of the actuator changes depending on the air pressure applied to it; therefore, the joint angle and stiffness are output by changing the combination of air pressures applied to the two actuators.

B. Actual control system

Fig. 5 shows a schematic of the system used to operate the antagonistic joint device created in this study. The device was controlled using a real-time system (MicroLabBox, dSpace). First, the desired joint angle and joint stiffness were input and substituted into the model, as shown in the block diagram in Fig. 4. Subsequently, the calculated air pressure was input into

a proportional solenoid valve to control the compressor. The air-pressure output from the compressor was applied to the actuator and the joint angle and stiffness were obtained. The output joint angle was measured using a rotary encoder. The air pressure applied to the actuator was measured using an air-pressure sensor, and the external torque applied was calculated using the tensile force measured using a load cell.

IV. Simulation

Simulations were performed to verify the air pressure required for each HEA to produce the target joint angle and stiffness.

The spring constants k_1 and k_2 were calculated by substituting the parameter values in Table I and results of the basic characteristics test of the actuator; the calculation was performed using the adjustment coefficient. The applied air pressure was set in the range of 0–300 kPa, the target joint angle in the range of -90–90 deg, and the target joint stiffness in the range of 0.0–0.3 Nm/rad with a step size of 0.1 Nm/rad. The results are shown in Fig. 6. The vertical axis represents the air pressure applied to the HEA [kPa], horizontal axis represents the target joint angle [deg], and slope represents the target joint stiffness [Nm/rad]. For example, to output a target joint angle of -30 deg and target joint stiffness of 0.2 Nm/rad, an air pressure of 126 kPa must be applied to actuator 1 and 186 kPa to actuator 2. Thus, the applied pressure can be uniquely determined by setting the target joint angle and stiffness.

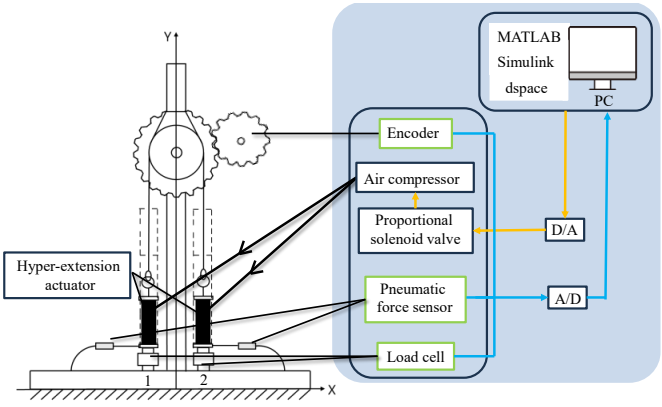

Figure 5. Control system for antagonistic joint devices.

TABLE I. Parameters In Model

Parameter	Value [unit]
A_1, A_2	0.483×10^{-8} [m^2]
k_1, k_2	1.1×10^{3} [N/m]
r	0.019 [m]
x_{01}, x_{02}	0.019×π [m]
θ_d	-90~90 [deg]
τ	0 [Nm]
K_{jd}	0~0.3 [Nm/rad]
a	5 [-]

V. Evaluation of Joint-Control Performance

In this section, we verify whether the specified joint angles and stiffness are outputted in the actual machine using model Equations (5) and (6).

A. Joint-angle control experiment

In this experiment, we verified whether the specified joint angles were output by the actual machine. First, we set the arm angle to 0 deg, inputted the target angle and air pressure calculated from the model to the actuator via a proportional solenoid valve, operated the arm until the rotary encoder-measurement value stabilized, and then returned it to 0 deg. At this time, the joint stiffness was maintained at 0.1 Nm/rad, and only the angle was varied under three conditions: 0–30–0 deg, 0–60–0 deg, and 0–90–0 deg. The number of trials was set to five for each condition.

The results of the joint-angle control experiments are shown in Fig. 7. Fig. 7(a) shows the results for the left side, i.e., the -90–0 deg ranges in Fig. 1 and Fig. 5, and Fig. 7(b) shows the results for the right side, i.e., the 0–90 deg range. The horizontal axis represents the commanded angle, and the vertical axis represents the output angle measured by the rotary encoder. The dashed lines represent the theoretical values. A comparison of the output angles of 30 deg, 60 deg, and 90 deg showed that the error range was approximately 5 deg for the commanded angle of 90 deg, and approximately 3 deg for the commanded angles of 30 deg and 60 deg. The error between the commanded and measured values in this case occurs because the spring constant of the actuator was derived using a first-order approximation rather than a third-order approximation, resulting in the failure to consider hysteresis. Furthermore, by setting the maximum air pressure applied to the actuator to 300 kPa this time, the joint angle range was set to -90 to 90 degrees. However, by increasing the applied air pressure in the future, an expansion of the usable joint angle range is anticipated.

B. Joint-stiffness control experiment

In this experiment, we verified whether the commanded joint stiffness was output by the actual machine. First, we set the commanded angle of the arm to 0 deg, inputted the commanded pressure to output the commanded stiffness, and operated the arm until the measured value of the rotary encoder became constant.

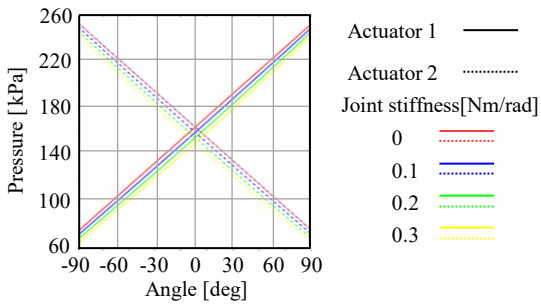

Figure 6. Calculated results of applied air pressure.

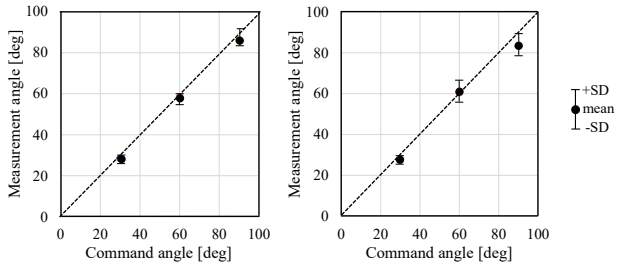

(a) Left (b) Right

Figure 7. Responsiveness of the joint angle.

TABLE II. Responsiveness Of Joint Stiffness

a) K_{jd} = 0.1 Nm/rad

Push In Angle [deg]	F' [N]		K_j [Nm/rad]	
	Mean	SD	Mean	SD
5	0.47	0.0047	0.103	0.00099
10	0.92	0.0052	0.101	0.00044
15	1.40	0.0046	0.102	0.00032

b) K_{jd} = 0.2 Nm/rad

Push In Angle [deg]	F' [N]		K_j [Nm/rad]	
	Mean	SD	Mean	SD
5	0.94	0.061	0.201	0.0061
10	1.85	0.029	0.202	0.0024
15	2.76	0.022	0.200	0.0015

c) K_{jd} = 0.3 Nm/rad

Push In Angle [deg]	F' [N]		K_j [Nm/rad]	
	Mean	SD	Mean	SD
5	1.35	0.033	0.296	0.0045
10	2.79	0.032	0.303	0.0030
15	4.23	0.053	0.306	0.0034

Once the measured value was constant, the tip of the arm was pushed at a specified angle perpendicular to the arm. The commanded joint stiffness was set to three values: 0.1, 0.2, and 0.3 Nm/rad. The commanded joint angle was kept constant at 0 deg, and the pushing angle was set to 5 deg, 10 deg, and 15 deg. Each condition was tested five times.The external force F'[N] applied to the arm during pushing was defined as the difference between actuators 1 and 2, and the external force F' was substituted into the following equation to calculate the joint stiffness K_j, which was then compared with the commanded joint stiffness:

$$K_j = F' \times \frac{r}{\theta} \tag{7}$$

Note that r is the radius of the pulley and θ is the push angle.

The results are summarized in Table II. These results show that the measured joint stiffness (0.1, 0.2, and 0.3 Nm/rad) matches the commanded joint stiffness. Furthermore, the simulation results derived from the model assumptions matched the actual applied air pressure. This consistency is attributed to the alignment between the model assumptions and experimental conditions as well as the simulation parameters appropriately reflecting the measured values. This demonstrates the validity of the constructed model and suggests that an efficient simulation-based evaluation is possible for future joint-stiffness prediction and design. This time, the verification range for joint stiffness was set between 0.1 and 0.3 Nm/rad. However, expanding the verification range in the future will likely enable the output of joint stiffness across a broader range.

VI. Conclusion

In this study, we developed an antagonistic joint based on a mechanical-equilibrium model using an HEA and evaluated its control performance. The proposed antagonistic joint uses two HEAs arranged in pairs to enable the control of the joint angle and stiffness. We described the operating principle and model equations and confirmed the control performance by comparing the commanded and measured values through simulation and joint-control experiments. The output joint angle and stiffness matched the commanded values.

Future challenges include changing the method used to calculate the spring constant of the actuator used in the model to a fitting method that considers the hysteresis characteristics of rubber to bring the output joint angle closer to the commanded value. Experiments can be conducted to verify whether the joint-stiffness output is the same as the theoretical value even when the command angle is changed. Moreover, the model can be improved to expand the range of joint stiffness that can be output. Furthermore, using the antagonistic joint developed in this study, a mobile robot capable of operating in the same space as humans may be developed.

References

[1] J. Arents and M. Greitans, "Smart industrial robot control trends, challenges and opportunities within manufacturing," *Applied Sciences*, vol. 12, no. 2, p. 937, 2022.

[2] T. I. Erdei, R. Krakó, and G. Husi, "Design of a Digital Twin Training Centre for an Industrial Robot Arm," *Applied Sciences*, vol. 12, no. 17, Art. no. 17, Jan. 2022.

[3] M. Xiloyannis *et al.*, "Soft robotic suits: State of the art, core technologies, and open challenges," *IEEE Transactions on Robotics*, vol. 38, no. 3, pp. 1343–1362, 2021.

[4] A. Ali, V. Fontanari, W. Schmoelz, and S. K. Agrawal, "Systematic Review of Back-Support Exoskeletons and Soft Robotic Suits," *Front. Bioeng. Biotechnol.*, vol. 9, Nov. 2021.

[5] M. Nishiura, A. Hatano, K. Nishii, and Y. Okumatsu, "Development of Low-Inertia Backdrivable Arm Focusing on Learning-Based Control," in *2022 IEEE/RSJ International Conference on Intelligent Robots and Systems (IROS)*, pp. 9642–9649, Oct. 2022.

[6] S. Dirven and A. McDaid, "A Systematic Design Strategy for Antagonistic Joints Actuated by Artificial Muscles," *IEEE/ASME Transactions on Mechatronics*, vol. 22, no. 6, pp. 2524–2531, Feb. 2017.

[7] W. Zhao and A. Song, "Active motion control of a knee exoskeleton driven by antagonistic pneumatic muscle actuators," in *Actuators*, MDPI, p. 134, 2020.

[8] T. Shin, T. Ibayashi, and K. Kogiso, "Detailed Dynamic Model of Antagonistic PAM System and Its Experimental Validation: Sensorless Angle and Torque Control With UKF," *IEEE/ASME*

Transactions on Mechatronics, vol. 27, no. 3, pp. 1715–1726, Jun. 2022.

[9] S. Tanaka, H. Nabae, and K. Suzumori, "Backstretchable mckibben muscles: Expanding the range of antagonistic muscle driven joints," *IEEE Robotics and Automation Letters*, 2023.

[10] H. Tomori, H. Oshika, T. Nakamura, H. Osumi, K. Hashimoto, and A. Nozawa, "Development and control of 1-DOF manipulator using electrostrictive rubber actuator," in *IECON 2013-39th Annual Conference of the IEEE Industrial Electronics Society*, IEEE, pp. 4085–4090, 2013.

[11] A. B. S. da Silva, G. E. P. Mendes, E. S. Bragato, G. L. Novelli, M. Monjardim, and R. M. Andrade, "Finger Prosthesis Driven by DEA Pairs as Agonist–Antagonist Artificial Muscles," *Biomimetics*, vol. 9, no. 2, Art. no. 2, Feb. 2024.

[12] N. G. Tsagarakis, S. Morfey, H. Dallali, G. A. Medrano-Cerda, and D. G. Caldwell, "An asymmetric compliant antagonistic joint design for high performance mobility," in *2013 IEEE/RSJ International Conference on Intelligent Robots and Systems*, IEEE, pp. 5512–5517, 2013.

[13] Z. Li *et al.*, "A novel cable-driven antagonistic joint designed with variable stiffness mechanisms," *Mechanism and Machine Theory*, vol. 171, p. 104716, May 2022.

[14] X. Chen, W. Zhu, W. Liang, Y. Lang, and Q. Ren, "Control of Antagonistic McKibben Muscles via a Bio-inspired Approach," *J Bionic Eng*, vol. 19, no. 6, pp. 1771–1789, Nov. 2022.

[15] F. Durante, M. G. Antonelli, P. B. Zobel, and T. Raparelli, "Development of a straight fibers pneumatic muscle," *International Journal of Automation Technology*, vol. 12, no. 3, pp. 413–423, 2018.

[16] K. Seno, T. Abe, and H. Tomori, "Development of 2-DOF Manipulator Using Straight-Fiber-Type Pneumatic Artificial Muscle for Agriculture," *Journal of Robotics and Mechatronics*, vol. 37, no. 1, pp. 64–75, 2025.

[17] D. Tanaka, D. Kamo, T. Watanabe, M. Maehara, and T. Nakamura, "Development of a 7-DOF manipulator actuated by straight-fiber-type pneumatic artificial muscle," in *2013 IEEE/ASME International Conference on Advanced Intelligent Mechatronics*, IEEE, pp. 300–306, 2013.

[18] T. Kawamura, K. Takanaka, T. Nakamura, and H. Osumi, "Development of an orthosis for walking assistance using pneumatic artificial muscle: A quantitative assessment of the effect of assistance," in *2013 IEEE 13th International Conference on Rehabilitation Robotics (ICORR)*, IEEE, pp. 1–6, 2013.

[19] P. Babaei Banyarani, B. Tarvirdizadeh, and A. Hadi, "Design and fabrication of a soft wearable robot using a novel *pleated fabric* pneumatic artificial muscle (pfPAM) to assist walking," *Sensors and Actuators A: Physical*, vol. 370, p. 115278, May 2024.

[20] F. Ito, T. Itsuno, and T. Nakamura, "MD-LUFFY: Massively Deformed Linearly-elongation-actuator Using Flexible Fiber and Yarn-Fundamental Characteristics on Elongation/contraction and Expansion rate," in *2024 IEEE International Conference on Advanced Intelligent Mechatronics (AIM)*, pp. 148–153, Jul. 2024.